The Astrophysical Journal, 587:544–550, 2003 April 20

A EUROPEAN SOUTHERN OBSERVATORY VERY LARGE TELESCOPE SURVEY OF NEAR-INFRARED ($Z \leq 25$) SELECTED GALAXIES AT REDSHIFTS $4.5 < z < 6$: CONSTRAINING THE COSMIC STAR FORMATION RATE NEAR THE REIONIZATION EPOCH[1]

A. Fontana,[2] F. Poli,[2] N. Menci,[2] M. Nonino,[3] E. Giallongo,[2] S. Cristiani,[3] and S. D'Odorico[4]
Received 2002 October 16; accepted 2002 December 13

ABSTRACT

We present the results of a Very Large Telescope (VLT) and *Hubble Space Telescope* imaging survey aimed at the identification of $4.5 < z < 6$ galaxies. In the VLT data, a set of broadband and intermediate-band filters has been used to select 13 high-z candidates in a $Z_{AB} \leq 25$ mag catalog, over an area of about 30 arcmin^2. Discrimination against lower redshift interlopers (mainly early-type galaxies at high redshift and cool Galactic stars) has been done combining morphological and spectral classification. This sample has been combined with a deeper $I_{AB} \leq 27.2$ mag sample obtained from the Hubble Deep Field (HDF) campaigns. The VLT final sample consists of 13 high-z candidates, four of which are identified with high confidence as $z > 4.5$ galaxies. The resulting integral surface density of the $Z_{AB} < 25$ candidates at $z > 4.5$ is in the range 0.13–0.44 arcmin^{-2}, and that in the highest redshift bin $5 < z \leq 6$ is between 0.07 and 0.13 arcmin^{-2}. In the two HDFs, we identify 25 galaxies at $I_{AB} \leq 27.2$ in the range $4.5 \leq z < 5$ and 16 at $5 \leq z \leq 6$, corresponding to surface densities of 3.1 and 2 arcmin^{-2}, respectively. We show that the *observed* $Z_{AB} < 25$ UV luminosity density (LD) appears to drop by about 1 order of magnitude from $z \simeq 3$ to 6. However, if we apply a threshold to obtain an absolute magnitude–limited sample, the UV LD is roughly constant up to $z \simeq 6$. We finally show that recent semianalytic hierarchical models for galaxy formation, while predicting a nearly constant *total* UV LD up to $z \simeq 6$, underpredict the observed UV LD at $Z_{AB} \leq 25$ and overpredict the $I_{AB} \leq 27.2$ one. This behavior can be understood in terms of a poor match to the slope of the UV luminosity function.

Subject headings: galaxies: distances and redshifts — galaxies: formation — galaxies: high-redshift

1. INTRODUCTION

Current findings on the production of the stellar baryon budget of the universe (Madau, Pozzetti, & Dickinson 1998) have shown a complex, gradual process, spread across a considerable fraction of the cosmological lifetime, rather than confined to a preferred epoch in the past. The evolution of the rest-frame ultraviolet luminosity density (LD) can be used to trace this process: since it is produced mainly by O, B short-living massive stars, it is almost independent of the star formation history of the galaxies (Madau et al. 1998), but it is tied to the fraction of the current star formation rate (SFR) not extincted by dust.

Measurements of the UV LD from the local environment up to $z \simeq 1$ show an increase with redshift (Lilly et al. 1996; Madau et al. 1998; Wilson et al. 2002). At the highest redshifts, where the results are often based on imaging surveys and photometric redshifts, the UV LD appears to be roughly constant between $z = 1$ and about 4 (Connolly et al. 1997; Pascarelle, Lanzetta, & Fernandez-Soto 1998; Fontana et al. 1999; Steidel et al. 1999; Lanzetta et al. 2002).

Here we focus on the redshift interval $z = 4.5$–6, a range that marks a critical phase in the history of the universe, when it was just emerging from the reionization epoch. Although first glances of the early universe have been made possible from the Sloan Digital Sky Survey that have provided the first statistically defined sample of quasars extending up to $z = 6.28$, the galaxy population at these epochs is presently nearly unexplored.

Indeed, it is at these very high redshifts that it is possible to set severe constraints on the physical mechanisms that drive the galaxy formation and evolution. The main goal behind the study of high-redshift galaxies is the construction of a coherent picture of the physical processes that led to galaxy evolution. Within the framework of gravitational instability driven by primordial fluctuation, simple but physically motivated prescriptions have been used over the last years to describe the main processes involved (e.g., White & Frenk 1991; Cole et al. 1994, 2000; Somerville & Primack 1999; Menci et al. 2002). These models are not as "tunable" as commonly believed since they cannot be modified freely to match the high-redshift observables without worsening the local fits (e.g., the local luminosity function or local Tully-Fisher relation). In this respect, any discrepancy between the model predictions and the observed properties reveals the lack or incorrect treatment of some fundamental processes. In this context, it is important to perform these comparisons directly at the highest redshifts, where the physical processes leading to present-day galaxies are caught in the act.

Despite the obvious interest in the field and the exciting results obtained at $z \simeq 3$ (Steidel et al. 1996), the discovery of galaxies at $z > 4.5$ has been so far serendipitous. There are obvious difficulties to tackle: First, the objects become progressively fainter and rarer. Second, the multicolor "dropout" criteria used to select high-z galaxies must be shifted from the UV-visual into the near-infrared (NIR)

[1] Based on observations obtained in service mode at the ESO VLT for the program 65.O-0445.

[2] Instituto Nazionale di Astrofisica, Osservatorio Astronomico di Roma, Sede di Monteporzio Catone, via Frascati 33, I-00040 Monteporzio, Italy.

[3] Instituto Nazionale di Astrofisica, Osservatorio Astronomico di Trieste, via G. B. Tiepolo 11, I-34131 Trieste, Italy.

[4] European Southern Observatory, Karl-Schwarzschild-Strasse 2, D-85748 Garching bei München, Germany.

bands to follow the rest-frame UV. For the same reasons, the spectroscopic follow-up is progressively harder. Besides this, the number of possible interlopers increases, with early-type galaxies and late-type stars progressively entering in the selection criteria. The current statistics of high-z galaxies reflects these problems. Few serendipitous objects have been identified (e.g., Spinrad et al. 1998), mostly because of a large equivalent width emission line identified as Lyα (e.g., Chen, Lanzetta, & Pascarelle 1999; Hu, Cowie, & McMahon 1998; Hu, McMahon, & Cowie 1999; Hu et al. 2002). Some identifications have been later disputed on the basis of deep imaging shortward of the (presumed) Lyman limit (Chen et al. 2000; Stern et al. 2000b). In general, the search of $z \geq 5$ emission-line galaxies has been shown to suffer from the strong contamination by O II emitters at $z \simeq 1.4$ (Stern et al. 2000a). Thus, the conclusions that can be drawn from the few objects observed so far are that (1) spectroscopy is by itself not conclusive at these redshifts to derive a firm estimate of the average cosmic SFR because it mostly requires the existence of a strong Lyα emission line and because of the contamination from O II emitters, and (2) deep imaging observations are required in any case not only to select the objects but also to validate the spectroscopic identifications.

Previous color selections at $z > 4.5$ based on the photometric redshift technique (Fontana et al. 1999) took advantage of the very deep Hubble Deep Field–North (HDF-N) and Hubble Deep Field–South (HDF-S) samples, discovering four $z > 5.5$ candidates in each field down to $I_{AB} < 27.5$. Evidence has come up for a comoving UV LD at $z \simeq 5$ lower by a factor of 5 than at $z \simeq 3$. However, this estimate is based on a sample of very faint sources selected in a small area and could be strongly affected by the presence of large-scale structure in the "pencil" beams.

For this reason, we have started a relatively deep survey of galaxies selected in the Z band to search for galaxies at $4.5 \leq z \leq 6.2$, covering two well-known fields where broadband multicolor imaging is available, namely, the extended ESO Imaging Survey (EIS) HDF-S and the New Technology Telescope (NTT) Deep Field (NDF). We have designed a strategy based on a combination of intermediate-band and broadband filters to identify high-z galaxies against the increasingly large number of interlopers. We emphasize that this is not a "preselection" survey, but it is designed to provide by itself a reliable identification for the bulk of the galaxy population at $z \geq 5$. To increase the accuracy of the photometric estimate of the redshift and to minimize the presence of interlopers (mainly intermediate-redshift early-type galaxies and late-type stars) in our high-z sample, we have included a set of intermediate-band filters, namely, IB691, IB834, and IB915, available at the ESO/VLT FORS imager. These filters, although of intermediate width, are relatively efficient since they sample spectral regions devoid of strong sky emission lines. The adopted filter set is thus tailored to trace the peculiar spectral features of the extremely high redshift galaxies, i.e., the flat rest-frame UV continuum that even at $z \sim 6$ can be sampled by the $Z-$IB915 color and the very abrupt change of the shape due to the hydrogen absorption spectral breaks by the intergalactic and interstellar medium sampled by the bluer bands.

In the following, we will adopt a ΛCDM cosmology with $\Omega_\Lambda = 0.7$, $\Omega = 1$, and $H_0 = 70$ km s^{-1} Mpc^{-1}. All magnitudes will be given in the AB system.

2. PHOTOMETRIC DATABASE AND THE SELECTION OF THE SAMPLE

The data set that we have analyzed consists of a composite sample of optical and infrared images centered on two public deep fields: a 16.3 arcmin^2 area around the ESO NDF (Arnouts et al. 1999) and a 13.6 arcmin^2 area around the HDF-S. The new data presented here have been obtained with the spectroimagers FORS1 and FORS2, at VLT-Antu and VLT-Keyun, respectively, in the R, IB691, I, IB834, Gunn z, and IB915 bands, and coupled with available UBV and NIR images obtained at NTT (Saracco et al. 1999; da Costa et al. 1998; Fontana et al. 2000). Details of the observations are given in Table 1.

Data reduction has followed the usual steps for deep imaging surveys in dithered mode, as described, for instance, in Fontana et al. (2000). Since fringing effects have been found to be significant in the reddest bands, we have applied special care in masking even the faintest objects

TABLE 1
SUMMARY OF THE OBSERVATIONAL DATA

	NDF			HDF-S		
FILTER	Instrument	Seeing	Magnitude Limit[a]	Instrument	Seeing	Magnitude Limit[a]
U.....	NTT-SUSI2	0.97	27.5	NTT-SUSI2[b]	1.02	28.3
B.....	NTT-SUSI2	1.26	28	NTT-SUSI2[b]	0.92	28.0
V.....	NTT-SUSI2	1.12	27.6	NTT-SUSI2[b]	1.04	28.1
R.....	VLT-FORS1	0.88	28.4	VLT-FORS1	0.86	27.9
IB691....	VLT-FORS1	0.55	28.1	VLT-FORS1	0.68	27.8
I.....	VLT-FORS1	0.81	27.4	VLT-FORS1	0.65	27.2
IB834....	VLT-FORS1	0.63	27.2	VLT-FORS1	0.82	26.6
z.....	VLT-FORS2[b]	0.65	27.1	VLT-FORS1	0.65	26.2
IB913....	VLT-FORS2[b]	0.65	26.4	...	...	...
J.....	NTT-SOFI[b]	0.77	25.7	NTT-SOFI[b]	1.04	25.8
H	...	...	...	NTT-SOFI[b]	1.03	24.43
K.....	NTT-SOFI[b]	0.7	25.1	NTT-SOFI[b]	1.06	24.87

[a] Computed in the AB system, at 1 σ, in 2″. Limiting magnitudes have been estimated from the photometric catalogs used in the paper and defined as the typical value at which $\Delta m = 1.08/3$.

[b] Public data, from http://www.eso.org.

prior to fringing removal. To account for the remaining sky residuals and the pixel-to-pixel correlation induced by dithering, we have adopted an estimation of the noise from sky variance inside a 3″ diameter aperture as described in Hu et al. (1999).

In the overall 29.9 arcmin^2 area common to the optical and IR observations, a photometric multicolor catalog of objects detected in the Gunn z band has been extracted following a recipe tailored to obtain accurate color photometry from ground-based images with different seeing conditions that we developed and tested on the imaging data of the K20 survey (Cimatti et al. 2002). Total magnitudes and colors have been estimated by the SExtractor code (Bertin & Arnouts 1996). For relatively bright objects, both the total flux in the Gunn z images and colors have been estimated from the MAG_AUTO magnitude.

For faint objects, we have used aperture magnitudes obtained by measuring fluxes within three increasing aperture diameters of 1″, 2″, or 3″ depending on the relative distance of the nearest source. In this case, an average correction (estimated on brighter galaxies) has been applied to account for seeing differences among different bands. The choice of apertures of 1″, 2″, and 3″ has been taken on the basis of the results obtained within the K20 data set, where we found that using apertures as large as 3″ (for isolated objects) still leads to an improvement in the accuracy of photometric redshifts. In the case of the present data, where the sample is deeper and the seeing of the detection image is better than the K20 K images, we verified that the results do not depend on the exact choice of the largest aperture. Indeed, we still select the same sample of $z \geq 4.5$ candidates and obtain similar estimates of the UV luminosity densities even using catalogs based on 2″ apertures, although the total magnitudes of individual objects may vary up to about 0.1 mag. We limit the following discussion to the $Z_{\rm AB} < 25$ subsamples.

The selection of high-z candidates has been performed using the complete multiband catalogs. The spectral features that identify high-redshift galaxies are the abrupt spectral breaks due to intervening and intrinsic H I absorption and the flat rest-frame UV continuum longward of Lyα. In particular, the H I absorption produces flux dropouts in the V, R, and even I bands as the redshift increases from $z = 4.5$ to 6. The selection of high-z candidates is usually done with color selection criteria sensitive to this pattern. In our case, because of the large number of filters adopted and the relatively wide redshift range covered, we have directly applied our photometric redshift code, which is described in detail in Giallongo et al. (1998) and Fontana et al. (2000). The only difference with respect to these papers is that we have used here a set of spectral templates obtained with the Pegase 2.0 code (Fioc & Rocca-Volmerange 1997), which we have found to provide accurate redshift estimation on ground-based data sets (Cimatti et al. 2002). As shown in Fontana et al. (1999, 2000), the selection of high-z candidates with photometric redshifts is at least as efficient as the simple "dropout" technique at $z \simeq 3$ and more efficient at higher z.

Potential contaminants of the selected subsample of $z_{\rm fit} > 4.5$ candidates might come by either early-type galaxies at $z > 1$ (that may mimic the large spectral breaks in the optical bands) or cool galactic stars that could mimic the main spectral features of galaxies in this redshift range, as shown by Fontana et al. (2000).

The contaminations from the first class of interlopers are easy to treat with our filter set, since early-type galaxies have very bright detections in the infrared J and K bands, so that they are automatically excluded by our photometric redshift code.

The cleaning of the sample from the second kind of interlopers has been achieved following a double selection criterion, based on both morphological and spectral information. Morphology has been taken into account using the SExtractor CLASS_STAR classification parameter (Bertin & Arnouts 1996), which sharply classifies the objects in our samples down to $Z_{\rm AB} \leq 24$. In addition, the stellar spectral library by Pickles (1998) has been used to compute the expected stellar colors in our filter sets, to provide additional spectroscopic criteria for the star-galaxy separation.

We have first obtained the exclusion of obvious bright stars from the sample by removing the objects at $Z_{\rm AB} \leq 24$ with CLASS_STAR ≥ 0.85: the objects removed by this criterion are also better fitted by stellar templates. We provide a check of the reliability of this morphology-based classification in Figure 1, where the best-fit galactic spectrum is shown along with a best-fit outcome from a library of stellar spectra for four out of the whole sample of CLASS_STAR > 0.85 and $Z_{\rm AB} \leq 24$ high-redshift candidates. After this selection we found no high-redshift candidate at this relatively bright magnitude cut.

In the fainter magnitude interval $24 < Z_{\rm AB} \leq 25$, 16 objects have been detected by our photometric redshift code as having $z > 4.5$. Here an automatic classification becomes less reliable, since morphology cannot be accurately estimated at these faint levels. These candidates have been therefore inspected visually, and morphological information has been complemented with a comparison between the best-fit χ^2 of the galactic template and the $\chi^2_{\rm STAR}$ of the stellar spectra.

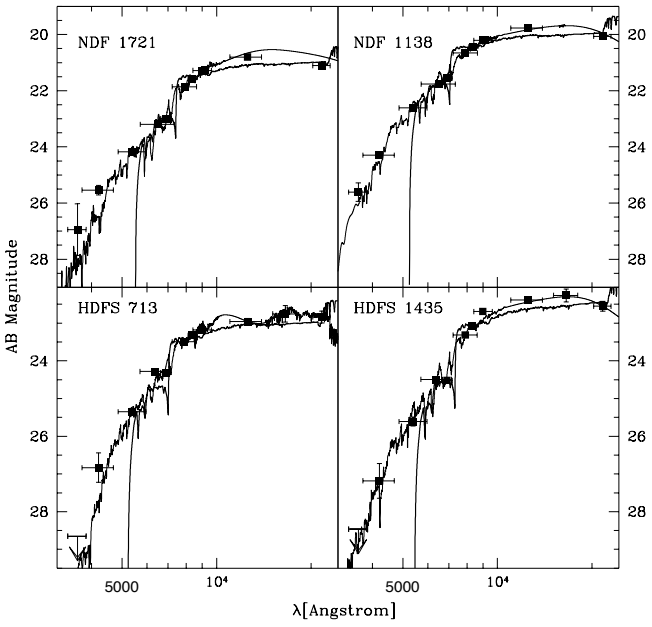

FIG. 1.—Best-fit spectral templates from the Rocca-Volmerange library (*thick line*) and from a library of stellar spectra (*thin line*) for a sample of CLASS_STAR > 0.85 and $Z_{\rm AB} \leq 24$ objects that we identify as Galactic stars.

From this analysis, we have singled out a "minimal" subsample of four sources that represent the most robust candidates showing clear extended morphological features, self-consistently detected in more than one band. On the other hand, three pointlike sources have been excluded as having stellar FWHMs in more than one band. For these objects, the spectral energy distribution is also more consistent with that predicted by the stellar library, i.e., $\chi^2_{\rm STAR} < \chi^2$. The remaining nine objects constitute the sample of candidates showing ambiguous characteristics, i.e., $\chi^2_{\rm STAR} > \chi^2$ but compact morphology or extended morphology but $\chi^2_{\rm STAR} < \chi^2$.

The spectral energy distribution of 12 out of our 13 candidates is shown for illustrative purpose in Figure 2, together with their best-fit galaxy templates. The crucial role played by intermediate-band filters is evident especially in those cases in which only upper limits or strongly uncertain values are available for the NIR J and K bands. In this way it is possible to sample the main features of these spectra, i.e., the strong drop shortward of the Lyman series absorption and the quite flat behavior longward of the same wavelength with an accuracy sufficient to discriminate between galaxies at $4.5 < z < 5$ and $5 < z < 6$.

In the following we will also use the photometric redshift sample of the WFPC2 HDF-N and HDF-S, presented in Fontana et al. (2000) and A. Fontana et al. (2003, in preparation), to select $z > 5$ galaxies at a deeper threshold of $I_{\rm AB} \leq 27.2$. For the HDF-S, the sample has been obtained from a new optical-IR catalog that uses ultradeep IR observations obtained with VLT-ISAAC. The catalog extraction procedure is described in Vanzella et al. (2001), while the final optical-IR photometric redshift catalogs are presented in A. Fontana et al. (2003, in preparation). In both cases, we will adopt an $I_{\rm AB} \leq 27.2$ selection criterion that ensures a small level of systematics in the estimated magnitudes (Vanzella et al. 2001). Combining the two HDF samples, we identify 25 galaxies at $I_{\rm AB} \leq 27.2$ in the range $4.5 \leq z < 5$ and 16 at $5 \leq z \leq 6$. A large variance still exists between the statistics in the two fields, with 17 (four) objects at $4.5 \leq z < 5$ ($z > 5$) in the HDF-S, against eight (12) in the HDF-N. A close-up of the HDF-S $z > 5$ candidates is shown in A. Fontana et al. (2003, in preparation).

We note that the new WFPC2 HDF-S catalog leads to major changes with respect to the one used in Fontana et al. (1999), which was based on the Stony Brook catalog (Lanzetta et al. 2002). In particular, three clear candidates at $z \geq 5.5$ that were absent in the previous catalog have been found at $I_{\rm AB} \leq 27.2$. We found that this comes from a systematic underestimate of the magnitudes at the faint levels in the Stony Brook catalog, which prevented these objects from being included in the $I_{\rm AB}$ selected catalog.

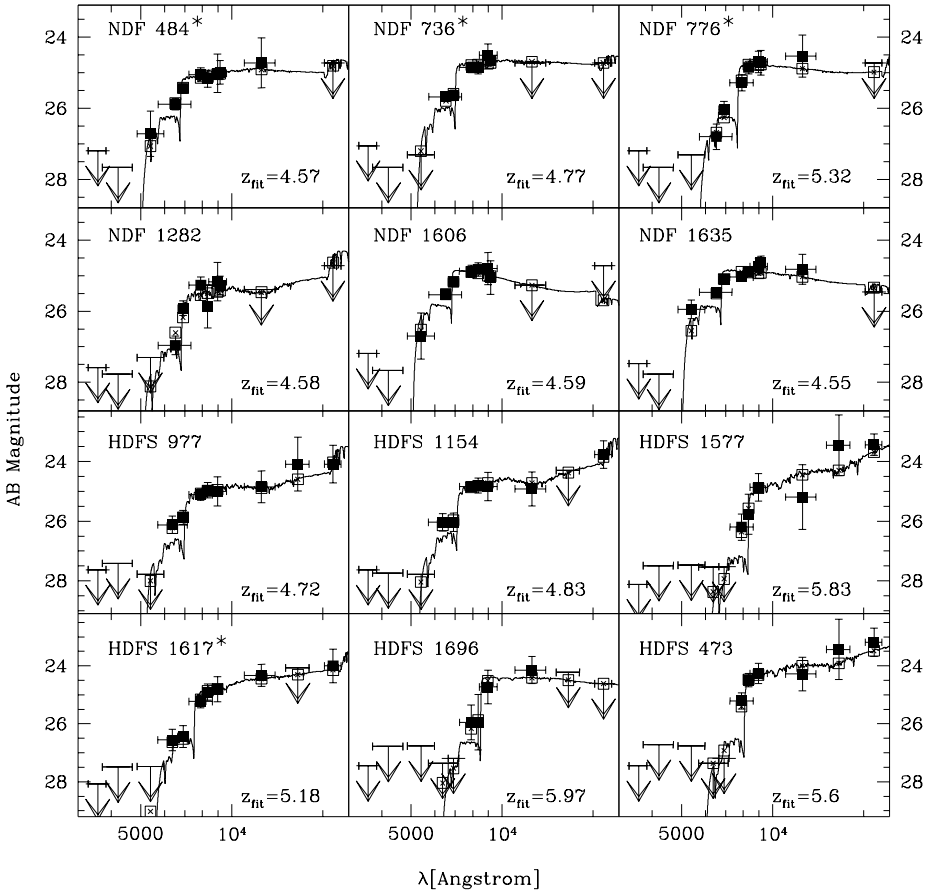

FIG. 2.—Best-fit spectral templates for 12 out of our 13 high-redshift candidates. Filled squares are measured AB magnitudes; 1 σ upper limit values are displayed as downward-pointing arrows. Open squares represent the mean value of the spectrum inside the filters. Objects with an asterisk belong to the "minimal" sample.

The resulting integral surface density of the $Z_{AB} < 25$ candidates at $z > 4.5$ is in the range 0.13–0.44 arcmin^{-2}, and that in the highest redshift bin $5 < z \leq 6$ is between 0.07 and 0.13 arcmin^{-2}. It should be emphasized that the stellar contamination of candidates at $z > 4.5$ ranges from a minimum of about 20% to a maximum of 75%. Thus, any estimate of the surface density of very high z protogalaxies should include a careful analysis of the contamination by the faint stellar population present in a given survey. In the two HDFs, the resulting surface densities at $I_{AB} \leq 27.2$ are 3.1 and 2 arcmin^{-2}, respectively.

Our lower and upper limits on the observed number densities at $Z_{AB} < 25$ and $5 < z \leq 6$ are 2–4 times higher than those predicted in the redshift range $5.5 < z \leq 6.5$ by Yan et al. (2002), who assumed that the shape of the luminosity function does not change from $z \simeq 3$ to 6. The slightly higher value that we find is mainly due to the lower normalization adopted by Yan et al. (2002), who chose to adopt 1.37 galaxies arcmin^{-2} at $I_{AB} \leq 27.2$, while we detect 2 galaxies arcmin^{-2}, and to the slightly lower redshift bin that we select. We also note that the ratio between the number densities measured at $Z_{AB} \leq 25$ and at $I_{AB} \leq 27.2$ is within a factor of 2 of that predicted by Yan et al. (2002), which may suggest that the slope of the UV luminosity function remains indeed unchanged from $z \simeq 3$ to 6.

3. EVALUATING THE OBSERVED AND PREDICTED UV LUMINOSITY DENSITY

We present in this section the UV LD resulting from our samples, using the usual $1/V_{max}$ formalism as described in Poli et al. (2001). Given the good agreement between data of the two fields, we compute the average UV LD of the total sample including both NDF and HDF-S objects, in the two redshift bins $4.5 < z \leq 5$ and $5 < z < 6$.

In both bins, the uncertainties due to possible stellar contamination are bracketed by the two triangles in the same redshift bin. The upward-pointing triangles represent the estimate derived from our minimal sample. The downward-pointing ones are derived from the total sample. Error bars are simply computed from Poisson statistics on the total number of galaxies in each bin following the recipe in Gehrels (1986) in the case of small numbers.

Although we are focusing on the two highest redshift bins, we have also computed the LD at $2.5 < z < 4.5$, to show its evolution on a complete $Z < 25$ sample. Again, photometric redshifts are estimated from the multiband observations, and stars have been excluded with a morphological and spectral classification similar to the one described above.

The *observed* quantities are shown in Figure 3*a*. As in Fontana et al. (1999), and at variance with other works, we have not corrected the observed values of the UV LD for incompleteness or extinction, but we explicitly show the differential effects of the inclusion of a magnitude limit and different dust extinction curves on the theoretical expectations that we will discuss below. To complement these observations, we present in Figure 3*b* the same quantities derived in the WFPC2 HDF-N and HDF-S $I_{AB} \leq 27.2$ samples.

At face value, the resulting picture is that the *observed* UV LD at $Z_{AB} < 25$ remains about constant in the redshift interval $2.5 < z < 4.5$ to values of the order of 10^{26} ergs s^{-1} Hz^{-1} Mpc^{-3} and then decreases by a factor of 10, reaching 10^{25} (average between our minimal and total sample of $5 < z < 6$ candidates).

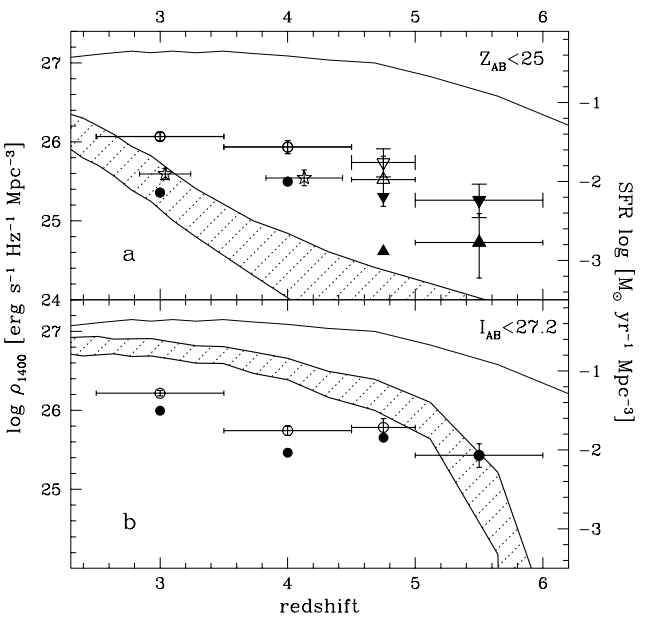

FIG. 3.—Observed and predicted UV luminosity densities as a function of redshift. (*a*) Data from our $Z_{AB} \leq 25$ survey. Upward-pointing triangles represent our estimates from the minimal sample, downward-pointing triangles those from the whole sample (see text for details). Open symbols represent the observed quantities. Filled symbols are the same quantities computed in a homogeneous sample that includes only objects down to the faintest absolute magnitude of the highest $z = 5$–6 sample (see text for details). Open stars represent the values from the Steidel et al. (1999) spectroscopic sample of galaxies at $R \leq 25$ shown for comparison. The continuous curves delimiting the shaded area represent the predictions at $Z_{AB} \leq 25$ by our fiducial model adopting different extinction curves for dust absorption. The thin curve shows the total UV (unobscured) LD associated with the total SFR of the fiducial model. (*b*) UV LD from the WFPC2 HDF-N/S sample of $I \leq 27.2$ galaxies. Symbol meaning and predicted curves are as in (*a*).

However, the comparison between the UV LD values computed in this way at different redshifts is prone to several biases. First, the $Z < 25$ or $I_{AB} \leq 27.2$ selection criterion results in a progressively brighter cutoff to the luminosity function at increasing redshifts.

Second, the rest-frame wavelength span by the Gunn z band ranges from 2250 Å at $z \simeq 3$ to 1300 Å at $z \simeq 6$, which may introduce color-dependent selection effects when computing the UV LD in the lowest redshift bins. The correction of both effects is uncertain, since it depends on the (largely unknown) shape of the luminosity function and color properties of the high-z galaxies.

In order to deal with these systematics in a clean way, we reproduce them in the theoretical predictions, as we describe below. A coarse correction of the varying luminosity cutoff is possible if we compute the UV LD limited at the faintest absolute magnitude of the highest $z = 5$–6 sample, i.e., at limiting fluxes of 1.2×10^{29} and 3.6×10^{28} ergs s^{-1} (corresponding to $M_{1400} \leq -19.8, -21.1$) in the Z- and I-selected samples, respectively. The corresponding values are shown with open symbols in both figures. The resulting picture is that the UV LD of the brightest galaxies is roughly constant from $z \simeq 3$ to 6. The values of the UV luminosity densities are given in Table 2.

TABLE 2
MEASURED UV LUMINOSITY DENSITY AT $z \geq 2.5$

	$\log \rho_{1400}$ (ergs s^{-1} Hz^{-1} Mpc^{-3})			
	VLT: $Z_{AB} \leq 25$		HDFs: $I_{AB} \leq 27.2$	
REDSHIFT	$Z_{AB} \leq 25$	$M_{1400} \leq -21.1$	$I_{AB} \leq 27.2$	$M_{1400} \leq -19.8$
3.....	26.07	25.36	26.22	26
4.....	25.94	25.5	25.74	25.47
4.75.....	25.52–25.74[a]	24.61–25.31[a]	25.78	25.65
5.5.....	24.73–25.26[a]	24.73–25.26[a]	25.43	25.43

[a] The two numbers correspond to the minimal and whole sample, as defined in the text.

4. DISCUSSION

In this work we have presented the results of a pilot survey aimed at detecting $z > 4.5$ galaxies with deep multicolor images. The key features of our approach are (1) the use of an extended set of broadband (*UBVRIZJK*) and intermediate-band ($\Delta\lambda \simeq 400$ Å) filters centered at 6900 and 8340 Å, (2) the adoption of conservative thresholds on the signal-to-noise ratio (S/N) for object detection, and (3) the application of morphological and spectral criteria; all these aspects improve the estimates of the redshifts and help exclude or minimize the number of lower z interlopers. When applied to the present data set, these criteria make it possible to reject all the brightest interlopers, which would dominate the LD, and to select a "minimal" sample of four high-confidence candidates at $z > 4.5$ and a sample of nine additional candidates where the stellar contamination is uncertain. This ambiguity depends on the relative depth of our data set: it is well within the possibilities of red-enhanced imagers at 8 m class telescope or of the Advanced Camera for Surveys to extend this kind of analysis 1–2 mag fainter, so that the stellar contamination to the LD can be lowered by a large amount, as in the case of the deeper but smaller WFPC2 HDF data that we present here.

Even with this ambiguity, the two selected data sets constrain the $z > 4.5$ UV LD with sufficient accuracy to show that the *observed* $Z_{AB} < 25$ UV LD drops by about 1 order of magnitude from $z \simeq 3$ to 6. This drop is largely due to the progressively brighter cutoff in the rest-frame luminosity function: if we correct for this incompleteness, the UV LD appears to be roughly constant from $z \simeq 2.5$ to 6.

The present results are apparently in contrast with recent findings by Lanzetta et al. (2002), who make use of the same WFPC2 HDF data and apply photometric redshifts that claim that the global SFR steadily increases up to $z = 12$. Unfortunately, the overall approach and techniques adopted are so different that it is difficult to make a clean comparison. First, we note that the use of wide-aperture magnitude and the adoption of a much higher S/N threshold to the catalog strongly reduce the systematics in the WFPC2 data induced by surface brightness dimming, which otherwise require the complex and model-dependent correction applied by Lanzetta et al. (2002). Besides, we draw our conclusions from a homogeneous sample that includes only objects selected down to the same absolute magnitude limit, rather than correcting for the incomplete coverage of the luminosity function, as done by Lanzetta et al. (2002). Finally, the photometric redshift distribution obtained by Lanzetta et al. (2002) is markedly different from our own and peaks at $z \simeq 0$, a factor that may lead to an overestimate of the faint end of the SFR distribution function that is used to correct the high-z data. Despite all these differences, it is to be noted that the two results are still consistent when the more conservative estimate of Lanzetta et al. (2002) is compared with our data in the appropriate redshift range $z \simeq 3$–6: given the overall uncertainties, both analyses suggest that UV LD is roughly constant in this redshift range.

The question that naturally arises is whether a constant UV LD up to $z \simeq 6$ may be compatible with the hierarchical scenario of galaxy formation. To discuss this point, we present in both panels of Figure 3 the UV LD predicted by the CDM semianalytic model described in Menci et al. (2002). This model is based on the Cole et al. (2000) recipes, with an additional improved treatment of aggregation of satellite galaxies in common dark matter halos. We first show that the *total* SFR derived from this model (*thin solid lines*) is nearly constant from $z \simeq 2$ to about 5 and then fades by only a factor of about 5 at $z = 6$.

To allow a fair comparison with our data, we have applied the effects of magnitude limit cut and dust extinction directly to the theoretical model. The effect is shown by the thick solid lines in Figures 3*a* and 3*b*. The shaded area shows the possible effects of dust extinction, ranging from no dust (*upper lines*) to SMC-like extinction curve (*lower lines*). Please note that the inclusion of dust correction effects in the theoretical model decreases the average UV LD with respect to the unextincted amount. It appears that while the CDM model broadly encompasses the observed values, it progressively underpredicts the LD observed in the bright $Z_{AB} < 25$ sample, while it overpredicts the LD observed in the faintest $I_{AB} < 27.2$ sample. This behavior can be understood in terms of a poor match to the slope of the UV luminosity function. At the brightest magnitudes, the CDM model underpredicts the number of bright sources, while it overpredicts the number of fainter sources dominating the deeper sample. This is analogous to what has already been found at $z \simeq 3$ and confirms a general trend of this version of CDM models to underpredict the amount of SFR in high-redshift massive objects (Somerville & Primack 2001; Poli et al. 2001; Menci et al. 2002; Cimatti et al. 2002).

The origin of this discrepancy is likely tied to the lack or to the oversimplified treatment of fundamental physical processes. Indeed, we remark that the basic recipes adopted

in this model already concur to enhance the SFR in high-redshift massive objects and that these aspects are further boosted with respect to the models that we used in Fontana et al. (1999). The SFR is computed as $\dot{M}_* = M_g/\tau_*$, where M_g is the amount of cool gas and the timescale τ_* is proportional to the dynamical time $\tau_{\rm dyn}$ and to the galaxy circular velocity V_c as $\tau_* = \epsilon_*^{-1}\tau_{\rm dyn}\left(V_c/200 \text{ km s}^{-1}\right)^{\alpha_*}$. Since both M_g and $1/\tau_{\rm dyn}$ increase with redshift and $\alpha_* = -1.5$, these models naturally predict that the SFR increases with redshift (for a given galaxy mass) and is more efficient in massive galaxies (at a given redshift). In addition, feedback effects are also a strong function of V_c, since they scale as $(V_c)^{-5.5}$, and again strongly favor the more massive objects. These basic recipes, combined with the effects of the biased process of galaxy formation induced by hierarchical merging, already conspire to boost at high z the SFR in massive objects, with respect to the less massive one.

In the present context, it is not possible to flatten the high-z luminosity function by simply changing the free parameters of the model, since one rapidly worsens the fit to the local observables (Cole et al. 2000).

Other physical processes that are important in the high-z universe are not included in our model. On the one hand, mechanical and ionizational feedback on the intergalactic medium by early galaxy and QSO formation is not included in our rendition, a process that is expected to quench the SFR in low-mass objects and hereby flatten the low-luminosity side of the LF. On the other hand, molecular cooling is efficient at high z and not included here. Another possibility that has been proposed is that the starburst efficiency increases during major mergers. These "starburst" models are known to increase the bright side of the LF at $z = 3$–4 (Somerville & Primack 1999) but require new additional free parameters to be introduced in the models and may become less efficient at $z > 5$, when major merging events are very rare. The challenge of the next years is to include all these processes in a self-consistent picture that reproduces the high-z observables.

The VLT data used in this work have been mostly obtained in the framework of the proposal 65.O-0445: we are grateful to the VLT operators and scientists that have performed the observations in service mode. The Gunn z observations of the NDF have been obtained during the Science Verification Phase of FORS2-VLT. *UBV* and IR images of the HDF-S have been obtained by the EIS. The *UBV* observations of the NDF were performed in SUSI-2 guaranteed time of the Observatory of Rome in the framework of the ESO–Rome Observatory agreement for this instrument. We thank the referee, R. Windhorst, for careful reading of the manuscript and useful comments.

REFERENCES

Arnouts, S., D'Odorico, S., Cristiani, S., Zaggia, S., Fontana, A., & Giallongo, E. 1999, A&A, 341, 641
Bertin, E., & Arnouts, S. 1996, A&AS, 117, 393
Chen, H.-W., Lanzetta, K. M., & Pascarelle, S. 1999, Nature, 398, 586
Chen, H.-W., Lanzetta, K. M., Pascarelle, S., & Yahata, N. 2000, Nature, 408, 562
Cimatti, A., et al. 2002, A&A, 392, 395
Cole, S., Aragon-Salamanca, A., Frenk, C. S., Navarro, J. F., & Zepf, S. E. 1994, MNRAS, 271, 781
Cole, S., Lacey, C., Baugh, C., & Frenk, C. 2000, MNRAS, 319, 168
Connolly, A. J., Szalay, A. S., Dickinson, M., SubbaRao, M. U., & Brunner, R. J. 1997, ApJ, 486, L11
da Costa, L. N., et al. 1998, A&A, submitted
Fioc, M., & Rocca-Volmerange, B. 1997, A&A, 326, 950
Fontana, A., D'Odorico, S., Poli, F., Giallongo, E., Arnouts, S., Cristiani, S., Moorwood, A., & Saracco, P. 2000, AJ, 120, 2206
Fontana, A., Menci, N., D'Odorico, S., Giallongo, E., Poli, F., Cristiani, S., Moorwood, A., & Saracco, P. 1999, MNRAS, 310, L27
Gehrels, N. 1986, ApJ, 303, 336
Giallongo, E., D'Odorico, S., Fontana, A., Cristiani, S., Egami, E., Hu, E., & McMahon, R. G. 1998, AJ, 115, 2169
Hu, E., Cowie, L. L., & McMahon, R. G. 1998, ApJ, 502, L99
Hu, E., Cowie, L. L., McMahon, R. G., Capak, P., Iwamuro, F., Kneib, J.-P., Maihara, T., & Motohara, K. 2002, ApJ, 568, L75 (erratum 576, L99)
Hu, E., McMahon, R. G., & Cowie, L. L. 1999, ApJ, 522, L9
Lanzetta, K., M., Yahata, N., Pascarelle, S., Chen, H., & Fernandez-Soto, A. 2002, ApJ, 570, 492
Lilly, S. J., Le Fevre, O., Hammer, F., & Crampton, D. 1996, ApJ, 460, L1
Madau, P., Pozzetti, L., & Dickinson, M. E. 1998, ApJ, 498, 106
Menci, N., Cavaliere, A., Fontana, A., Giallongo, E., & Poli, F. 2002, ApJ, 575, 18
Pascarelle, S. M., Lanzetta, K. M., & Fernandez-Soto, A. 1998, ApJ, 508, L1
Pickles, A. J. 1998, PASP, 110, 863
Poli, F., Menci, N., Giallongo, E., Fontana, A., Cristiani, S., & D'Odorico, S. 2001, ApJ, 551, L45 (erratum 551, L127)
Saracco, P., D'Odorico, S., Moorwood, A., Buzzoni, A., Cuby, J.-G., & Lidman, C. 1999, A&A, 349, 751
Somerville, R. S., & Primack, J. R. 1999, MNRAS, 310, 1087
Spinrad, H., Stern, D., Bunker, A., Dey, A., Lanzetta, K. Yahil, A., Pascarelle, S., & Fernandez-Soto, A. 1998, AJ, 116, 2617
Steidel, C. C., Adelberger, K. L., Giavalisco, M., Dickinson, M., & Pettini, M. 1999, ApJ, 519, 1
Steidel, C. C., Giavalisco, M., Pettini, M., Dickinson, M., & Adelberger, K. L. 1996, ApJ, 462, L17
Stern, D., Bunker, A., Spinrad, H., & Dey, A. 2000a, ApJ, 537, 73
Stern, D., Eisenhardt, P., Spinrad, H., Dawson, S., van Breugel, W., Dey, A., de Vries, W., & Stanford, S. A. 2000b, Nature, 408, 560
Vanzella, E., et al. 2001, AJ, 122, 2190
White, S., & Frenk, C. S. 1991, ApJ, 379, 52
Wilson, G., Cowie, L. L., Barger, A. J., & Burke, D. J. 2002, AJ, 124, 1258
Yan, H., Windhorst, R. A., Odewhan, S. C., & Cohen, S. H. 2002, ApJ, 580, 725